Electronic Supplementary Material (ESI) for New Journal of Chemistry.

Bifunctional $NiCo_2S_4$/reduced graphene oxide@polyaniline nanocomposite as a highly-efficient electrode for glucose and rutin detection

Yanying Wang[1], Ji Zhong[1], Fang Ding[2], Qingbiao Zhao[3],Zhaoyi zhang[1], Xin Liu[1], Yiting Liu[1], Hanbing Rao[1*], Ping Zou[1], Xianxiang Wang[1]

1.College of Science, Sichuan Agricultural University, Ya'an 625014, China, P.R.China

2. Suzhou Institute of Systems Medicine, Suzhou, Jiangsu 215123, China；Center for Systems Medicine, Institute of Basic Medical Sciences, Chinese Academy of Medical Sciences & Peking Union Medical College, Beijing 100005, China, P.R.China

3.Key Laboratory of Polar Materials and Devices, Ministry of Education, Department of Electronic Engineering, East China Normal University, Shanghai, 200241 P.R. China

The authors wish it to be known that, in their opinions, Yanying Wang and Ji Zhongshould be regarded as joint First Authors.

Corresponding author :

Dr. Hanbing Rao

College of Science, Sichuan Agricultural University, Xin Kang Road, Yucheng District, Ya'an 625014, China, P.R. China.

E-mail addresses: rhb@sicau.edu.cn

Fig. S1

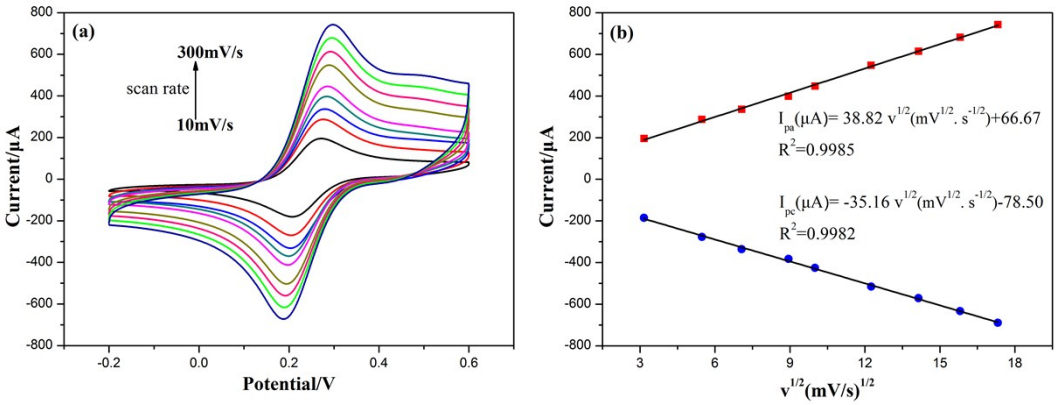

Fig. S1 (a) CVs of $NiCo_2S_4$/rGO@PANI/GCE in 5 mM $[Fe(CN)_6]^{3-/4-}$ with 0.5 M KCl at different scan rate (from 10 to 300 mV/s), (b) The linear relationship between peak currents and the square root of the scan rate.

Fig. S2

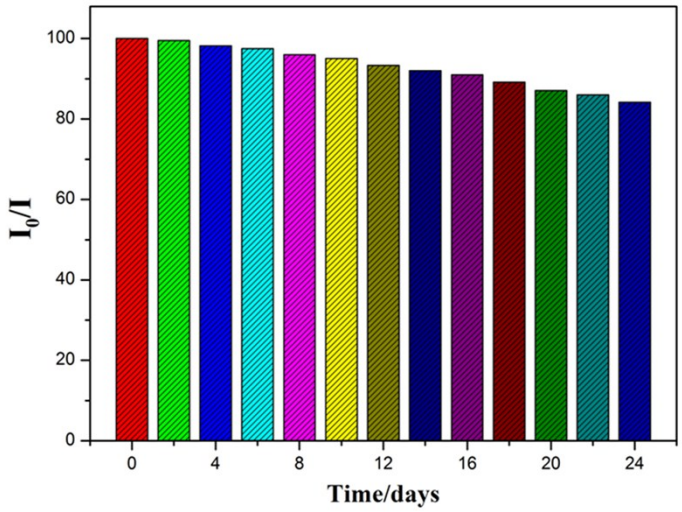

Fig. S2 Stability of the sensor stored under ambient conditions among 24 days using 0.1 M NaOH with 3 mM glucose.

1 Apparatus

XRD patterns were measured on a D/Max-RA Diffractometer (DX-2700, Dan Dong, China) with Cu Kα-radiation (λ=0.1548nm) operated at 40 kV and 100 Ma. TGA analysis was performed with a TGA209F3A Tarsus instrument (NETZSCH-

Gerätebau GmbH, Germany). SEM pictures were obtained from a JSM4800F instrument (JEOL, Japan) and TEM pictures were acquired at the JEOL2100F (JEOL, Japan). XPS analysis was carried on an ESCALAB 250Xi (Boyue, Shanghai, China). FT-IR spectra were recorded on a FTIR-8400s spectrometer (SHIMADZU, Japan) by using pressed KBr pellets.

2 Materials and reagents

Graphite powder (325 mesh, ≥99.85%) was purchased from Huayuan Chemical Co., Ltd. (Shanghai, China) Sodium nitrite ($NaNO_3$, ≥99.0%), sulfuric acid (H_2SO_4, 95.0-98.0%), hydrogen peroxide (H_2O_2, ≥30.0%), cobalt nitrate hydrate ($Co(NO_3)_2·6H_2O$, ≥98.5%), sodium chloride (NaCl, ≥99.5%), nickel nitrate hydrate ($Ni(NO_3)_2·6H_2O$, ≥98.0%), urea ($CO(NH_2)_2$, ≥99.0%), sodium sulfide ($Na_2S·9H_2O$, ≥98.0%), aniline (C_6H_7N, ≥99.5%), hydrochloric acid (HCl, 36.0-38.0%), potassium permanganate ($KMnO_4$, ≥99.5%), ammonium persulfate (APS, $(NH_4)_2S_2O_8$, ≥98.0%), ethanol (C_2H_5OH, ≥99.7%), potassium hexacyanoferrate ($K_3[Fe(CN)_6]$, ≥99.5%), sodium hydroxide (NaOH, ≥98.0%), potassium hexacyanoferrate trihydrate ($K_4[Fe(CN)_6]·3H_2O$, ≥99.5%), potassium chloride (KCl, ≥99.5%), potassium sulphate (K_2SO_4, ≥99.0%), sodium carbonate (Na_2CO_3, ≥99.0%), calcium chloride ($CaCl_2$ ≥96.0%), trisodium citrate ($C_6H_5Na_3O_7·2H_2O$, ≥99.0%), zinc chloride ($ZnCl_2$, ≥98.0%), iron trichloride ($FeCl_3$, ≥99.0%),ammonium phosphate ($(NH_4)_3PO_4$, ≥98.0%), hydroquinone (HQ, $C_6H_6O_2$, ≥98.0%), sodium dihydrogen phosphate (NaH_2PO_4 ≥99.0%), maltose ($C_{12}H_{22}O_{11}·H_2O$, 95.0%), disodium hydrogen phosphate (Na_2HPO_4 ≥99.0%), ascorbic acid (AA, $C_6H_8O_6$, ≥99.7%), glucose ($C_6H_{12}O_6$, analytical reagent), fructose ($C_6H_{12}O_6$, ≥99.0%), uric acid (UA, $C_5H_4N_4O_3$, ≥99.0%) and sucrose ($C_{12}H_{22}O_{11}$, analytical reagent) were purchased from Kelong Chemical Reagent Factory. (Chengdu, China). Rutin ($C_{27}H_{30}O_{16}$, ≥98.0%) was purchased from Darui Fine Chemicals Co., Ltd. (Shanghai, China). Acetaminophen ($C_8H_9NO_2$), quercetin ($C_{15}H_{10}O_7$, 97.0%), morin ($C_{15}H_{10}O_7$, >95.0%), galactose ($C_6H_{12}O_6$, 98.0%), trehalose ($C_{12}H_{22}O_{11}·2H_2O$, ≥99.0%) and dopamine (DA, $C_8H_{11}NO_2$, 98.0%) were purchased from Macklin Biochemical Co., Ltd. (Shanghai, China). All reagents were of analytical grade and all solutions were formulated with deionized water (18.2 MΩ·

cm^{-1}).

3 Preparation of electrodes and electrochemical characterization

All electrochemical tests were performed by using a CHI660E Electrochemical Workstation (Shanghai Chen Hua, China) at ambient temperature with an orthodox three-electrode system containing a GCE (with or without modification, Φ=3 mm) as the working electrode, saturated calomel electrode (SCE), and platinum (Pt) wire electrode as the reference and counter electrode, respectively. GCE, SCE, and Pt were obtained from Tianjin Incole Union Technology Co., Ltd. (Tianjin, China). Before the electrochemical tests, the alumina powders were used to polish the GCE, then the sonication was employed to clean the GCE. Ultimately, the homogeneous dispersions of obtained samples (0.5 $mg \cdot mL^{-1}$, 10 μL) were dropped on the GCE and dried in air.

4 FT-IR analysis and TGA

The molecular structures of the $NiCo_2S_4$/rGO and $NiCo_2O_4$/rGO@PANI nanocomposites were ascertained using FT-IR analysis within the wave-length range from 400 to 4000 cm^{-1} and the thermostability of these composites was examined by TGA in the temperature range from 40 °C to 900 °C under condensed Ar with a rate of 10 °C/min. These characterizations can further indicate that the formation of PANI on the $NiCo_2S_4$/rGO composite. **Fig. S3(A)** exhibited the FT-IR spectra of $NiCo_2S_4$/rGO and $NiCo_2O_4$/rGO@PANI, in the case of $NiCo_2S_4$/rGO, the peaks around 1102 cm^{-1}, 1624 cm^{-1}, 2852 cm^{-1}, 2922 cm^{-1} and 3425 cm^{-1} were vested in C-O-C, aliphatic C=C, the asymmetric stretching and symmetric vibrations of C-H and O-H bonds of rGO, correspondingly [1]. For $NiCo_2O_4$/rGO@PANI (**Fig. S3A(b)**), compared with $NiCo_2S_4$/rGO, a few new peaks can be observed since the existence of PANI, the new peaks locating in 1478 cm^{-1} and 1560 cm^{-1} were attributed to the characteristic C-C stretching of the benzenoid and quinonoid rings, respectively. Meanwhile, the peaks at 1241 cm^{-1} and 1296 cm^{-1} belonged to C=N and C-N stretching vibrations, respectively, the peaks at 796 cm^{-1} and 1108 cm^{-1} were assigned to the out-of-plane bending and in-plane bending of C-H, respectively [2].

Fig. S3(B) displayed the TGA thermograms of $NiCo_2S_4$/rGO and $NiCo_2O_4$/rGO@PANI composites. As seen from the **Fig. S3B(a)**, the primary weight

loss of $NiCo_2S_4$/rGO happened below 300 °C was ascribed to the absorbed water. Then, a slower weight loss between 300 and 650 °C result from the decomposition of the oxygen-containing functional groups and the destruction of carbon skeleton of rGO framework [3, 4]. In addition, $NiCo_2S_4$/rGO displayed a good thermal stability with a weight loss about 25% until 900 °C. Compared to $NiCo_2S_4$/rGO, the $NiCo_2O_4$/rGO@PANI underwent three-step thermal degradation process, the first small weight loss between 40 and 130 °C was caused by the remove of water as well as the low molecular weight oligomers. The next step weight loss in the temperature range from 150 to 300 °C was corresponded to the dopant HCl molecules loss, resulting in deprotonation of the PANI. And the main weight loss in the final step from 300 to 700 °C was attributed to the decomposition of PANI backbone chains [5, 6], with the thermal destruction of rGO. Obviously, the weight loss of $NiCo_2O_4$/rGO@PANI from 40 °C to 900 °C was around 40%.

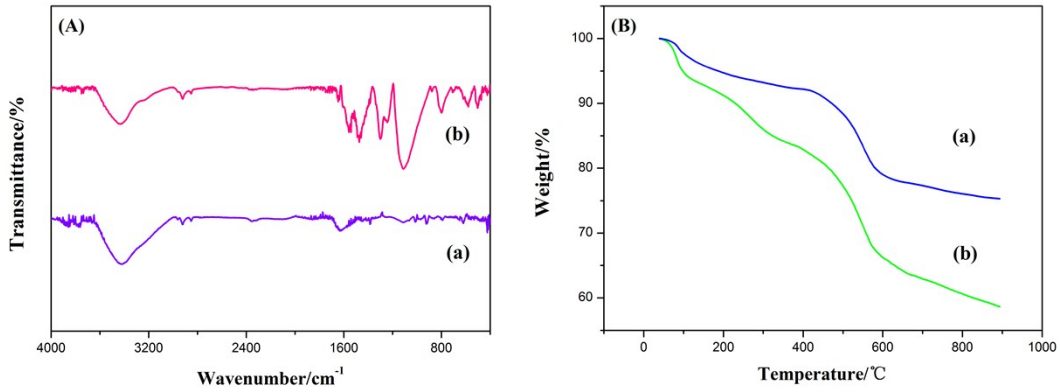

Fig. S3 (A) FT-IR spectra and (B) The TGA thermograms of (a) $NiCo_2S_4$/rGO, (b)$NiCo_2S_4$/rGO@PANI.

5 Electrochemical measurements of glucose

5.1 Effect of scan rate

The electrochemical mechanism information can be found in the relation between the scan rate and peak current. **Fig. S4(a)** exhibited the effect of scan rates on the electrocatalysis of 3 mM glucose in 0.1 M NaOH at the $NiCo_2S_4$/rGO@PANI electrode. Both the anodic and cathodic peak currents were enhanced with the increase of scan rate (between 10 to 300 mV/s). Moreover, the anodic peaks showed the significantly positive shift while the cathodic peaks shifted negatively as the scan

rate increasing. **Fig. S4(b)** revealed that the measured redox peak currents (μA) had a linear correlation with the scan rate (mV/s), and the linear regression values (R^2) were 0.9951 for anodic peak currents and 0.9942 for the cathodic peak currents, indicating that the glucose oxidation was a typical diffusion-controlled electrochemical process [7].

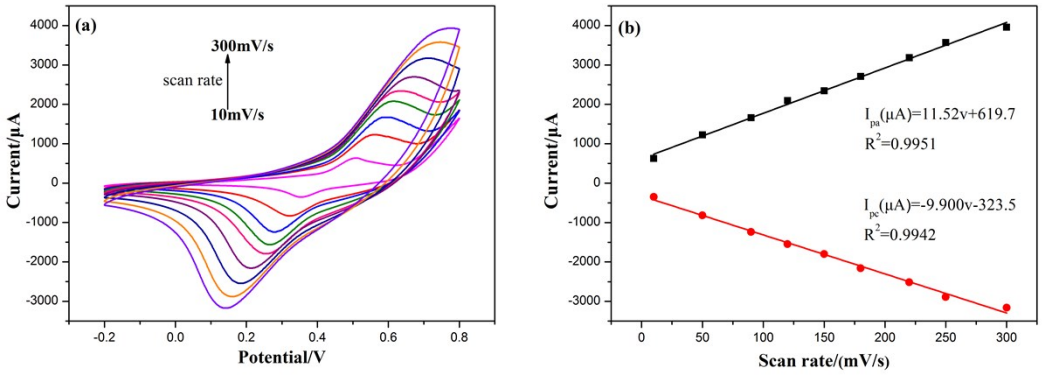

Fig. S4 (a) CV plots of the $NiCo_2S_4$/rGO@PANI electrode in 3 mM glucose at different scan rate (from 10 to 300 mV/s), (b) Plot of the peak currents of $NiCo_2S_4$/rGO@PANI anodic peak (black line), and cathodic peak (red line) vs. scan rate.

5.2 Effect of the working potential

It is well known that the amperomeric response is usually estimated by measuring the current at immovable working potentials in the existence of a particular determinand. Thus, to select the optimal working potential for the non-enzymatic electrochemical glucose sensing is extremely necessary. As shown in **Fig. S5(a)**, the amperometric response of $NiCo_2S_4$/rGO@PANI with the consecutive additions of glucose (100 μM) at varied working potentials of 0.50 V, 0.55 V as well as 0.60 V. There was almost obvious current difference between different potentials, and the figure displayed that the sensor showed a most excellent performance when the potential was under 0.55 V. In addition, the working potential at 0.55 V was similar to the oxidation peak potential (**Fig. 5A**) attained from the cyclic voltammogram. Consequently, the following experiments chose 0.55 V as the optimum working potential. After the glucose added, a notable enhancement of current response was rapidly obtained and the steady-state current (95% of the maximum value) was achieved within 4 s (**Fig. S5(b)**), this electrode exhibited a rapider response time for

the determination of glucose revealing the outstanding electrocatalytic activity and the quick electron exchange response of the $NiCo_2S_4$/rGO@PANI composite.

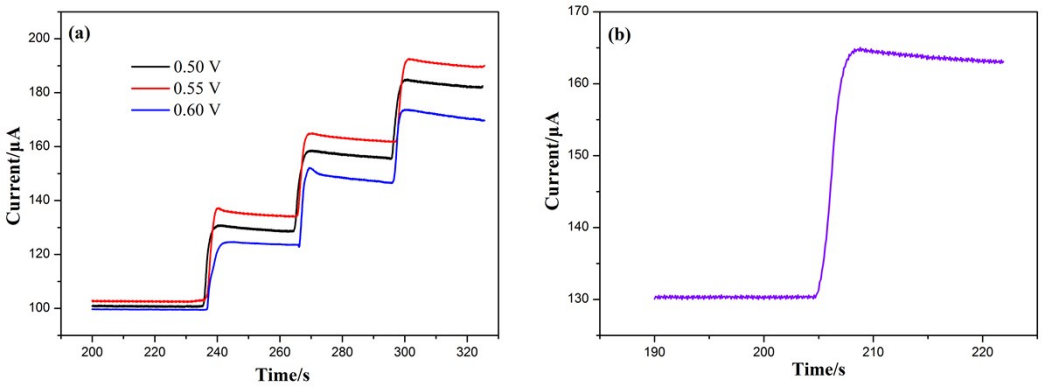

Fig. S5 (a) Amperometric current responses of $NiCo_2S_4$/rGO@PANI at various working potentials with every successive addition of 100 μM glucose, and (b) plot of response time.

6 Electrochemical measurements of rutin

6.1 Effect of pH

As is known to all that the experimental results can be effectively affected by the pH value of tested solutions. The effects of pH on the peak currents and peak potentials of 10 μM rutin in 0.1 M PBS at $NiCo_2S_4$/rGO@PANI were investigated by DPV with a pH variation from 1 to 6. According to the **Fig. S6(a),** the anodic peak currents (I_{pa}) of rutin increased with the increasing of pH from 1 to 3, and then decreased gradually with the pH further increasing. When the pH was attained 6, the I_{pa} became very small. Meanwhile, the anodic peak potential shifted towards to the low potential with the increasing pH value, manifesting that protons were involved in the electrooxidation of rutin [8]. Further plotted in **Fig. S6(b)**, the linear relationship between the E_{pa} and pH was presented as E_{pa} (V) = -0.06139pH + 0.6652 (R^2=0.9967). The slope of the regression equation was close to the theoretical value of -0.0591 V/pH at 25 °C, evincing that the electrochemical reaction possesses an equal number of electrons and protons taking part in it [9].

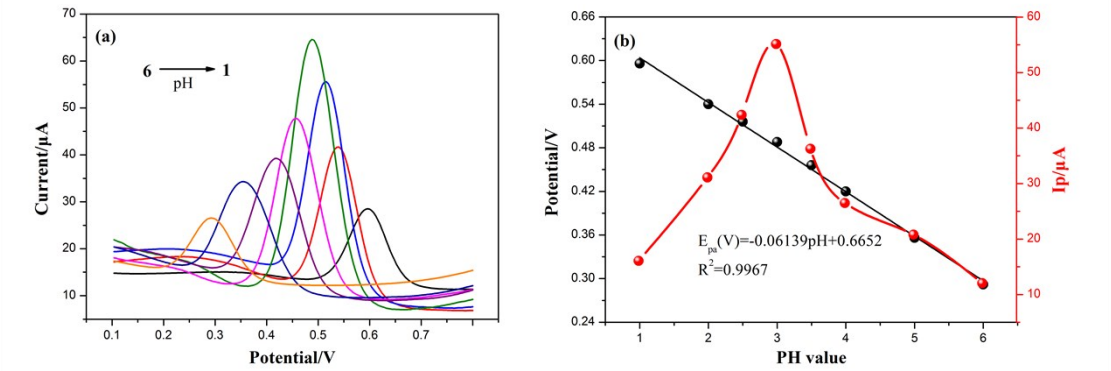

Fig. S6 (a) DPVs of 10 μM rutin in PBS with different pH value (pH: from 1 to 6), (b) Effect of pH on the anodic peak currents and potentials of 10 μM rutin. Amplitude: 0.05V, pulse width: 0.06s, increment: 0.004V.

6.2 Reproducibility and stability of the $NiCo_2S_4$/rGO@PANI modified electrode for rutin determination

The reproducibility of this sensor was performed in 0.1M PBS (pH = 3) with 10 μM rutin by DPV to evaluate the serviceability of proposed method. The reproducibility data for the oxidation peak currents of six similar $NiCo_2S_4$/rGO@PANI modified electrodes was shown in **Fig. S7(a)**. Comparing the change of peak current values, the RSD for detection of rutin was calculated as 3.27 %, which denoted a good reproducibility of the $NiCo_2S_4$/rGO@PANI modified electrode.

The long-term stability of the $NiCo_2S_4$/rGO@PANI modified electrode was investigated by testing the oxidation current responses of 10 μM rutin in 0.1 M PBS (pH = 3) using DPV measurement among 20 days. Before the electrochemical measurement, this electrode was stored under ambient conditions. As shown in **Fig. S7(b)**, 20 days later, the results indicated that the peak current response to rutin persisted 83.7% of the primary value, proving the outstanding storage and high chemical stability of the $NiCo_2S_4$/rGO@PANI electrochemical sensor.

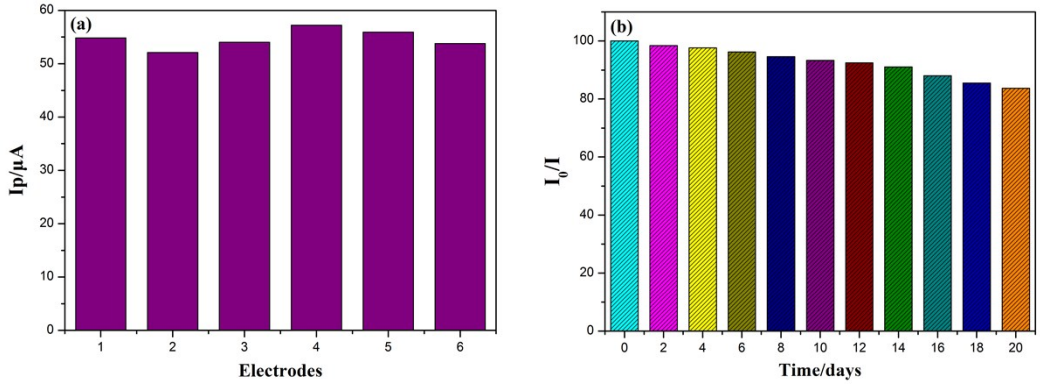

Fig. S7 (a) DPV response to rutin at six $NiCo_2S_4$/rGO@PANI modified electrodes prepared in the same conditions, (b) Stability of the sensor stored under ambient conditions for 20 days using 0.1 M PBS (pH = 3) with 10 μM rutin.

Table S1 Results of interference study on the response of rutin.

Interference	Concentration (μM)	Signal change (%)
$FeCl_3$	1000	0.98
K_2SO_4	1000	-0.45
$NaNO_3$	1000	1.03
$CaCl_2$	1000	-0.64
$ZnCl_2$	1000	-0.58
$(NH_4)_3PO_4$	1000	-1.26
Trisodium citrate	100	1.14
Uric acid	100	1.32
Acetaminophen	100	2.79
Hydroquinone	100	3.81
Ascorbic acid	100	4.32
Dopamine	100	4.73
Glucose	100	1.54
Quercetin	100	5.61
Morin	100	4.52

References

1. A. A. Ensafi, R. Noroozi, A. N. Zandi and B. Rezaei, *Sens. Actuator B-Chem.*, 2017, **245**, 980-987.
2. N. Chen, Y. Ren, P. Kong, L. Tan, H. Feng and Y. Luo, *Appl. Surf. Sci.*, 2016, **392**, 71-79.
3. H. Rao, Z. Zhang, H. Ge, X. Liu, P. Zou, X. Wang and Y. Wang, *New J. Chem.*, 2017, **41**, 3667-3676.
4. S. Sakthinathan, S. Kubendhiran, S. M. Chen and P. Tamizhdurai, *RSC Adv.*, 2016, **6**, 56375-56383.
5. H. Rao, C. Min, H. Ge, Z. Lu, L. Xin, Z. Ping, X. Wang, H. Hua, X. Zeng and Y. Wang, *Biosens. Bioelectron.*, 2017, **87**, 1029-1035.
6. N. Parveen, N. Mahato, M. O. Ansari and M. H. Cho, *Compos. Part. B.*, 2016, **87**, 281-290.
7. S. Liao, S. Lu, S. Bao, Y. Yu and M. Wang, *Anal. Chim. Acta*, 2016, **905**, 72-78.
8. H. Zhang, Q. Huang, Y. Huang, F. Li, W. Zhang, C. Wei, J. Chen, P. Dai, L. Huang and Z. Huang, *Electrochim Acta.*, 2014, **142**, 125-131.
9. C. E. Zou, B. B. Yang, D. Bin, J. Wang, S. M. Li, P. Yang, C. Q. Wang, Y. Shiraishi and Y. K. Du, *J. Colloid Interface Sci.*, 2017, **488**, 135-141.